"Solid lipid nanoparticles with docetaxel inside stop 4T1 mouse mammary cancer cells from developing tumors and spreading to the lungs."

Vinod D. Usnale* 1 Rohit D. Usnale 2, Ravi.R.More 3, Dr.Jyotiram A Sawale, 4.Dr.Reenu Yadav, 5.Dr.Jitendra Malviya

[1,2,3,4] Department of Pharmacy, IES Institute of Pharmacy,Bhopal (MP)

Abstract

Background: The majority of breast cancer-related fatalities in women are caused by metastasis. Here, utilizing 4T1-bearing BALB/c mice, we examined the anti-tumor effects of solid lipid nanoparticles (SLN-DTX) when utilized in the treatment of metastatic breast cancers.

Results:

By employing high energy, solid lipid nanoparticles (SLNs) were created. To stabilize nanoparticle dispersion, Compritol 888 ATO was used as the lipid matrix and Pluronic F127 and Span 80 as the surfactants. For at least 120 days, the particles had a high level of stability. The SLNs have a 128 nm dispersion size, a 0.2 polydispersity index (PDI), and a negative zeta potential. SLNs had a regulated drug release profile, high docetaxel (DTX) entrapment efficiency (86%), and drug loading of 2%. After 24 hours of treatment, SLN-DTX's half-maximal inhibitory concentration (IC50) against 4T1 cells was more than 100 times lower than that of free DTX. SLNDTX was substantially more effectively absorbed into the cells during the cellular absorption test than free DTX. When comparing cells treated with SLN-DTX (73.7%) to cells treated with free DTX (23.0%), which thereafter caused apoptosis, the accumulation in the G2M phase was much higher in the former group of cells. According to TEM research, endocytosis is the mechanism by which SLN-DTX internalization occurs, and fluorescence microscopy demonstrated that DTX caused microtubule damage. Studies conducted in animals revealed that SLN-DTX had stronger anticancer effectiveness than free docetaxel by decreasing tumor volume (p 0.0001) and preventing spontaneous lung metastasis in mice with 4T1 tumors. Lung histological tests proved that SLNDTX therapy could stop tumor growth. When taken as a combination therapy, IL-6 serum levels, ki-67, and BCL-2 expression all demonstrated a strikingly significant reduction.

Conclusions: According to our findings, DTX-loaded SLNs may be a potential delivery system for the treatment of breast cancer and the prevention of metastasis.

Keywords: *Cellular uptake, 4T1, NIH-3T3, IL-6, BCL-2, Ki-67 and antitumor effect*

Background:

The most common malignant tumor in women and the leading cause of death for women worldwide is breast cancer. The majority of breast cancer-related deaths are brought on by metastasis. Chemotherapy is used to increase patient survival time and stop metastasis and recurrence [1]. Chemotherapies used in these situations include taxanes (docetaxel or paclitaxel) [2].Docetaxel (DTX) is a semi-synthetic taxane that is generated from the European tree Taxus baccata and is a lipophilic anticancer agent [3]. Docetaxel has been licensed by the Food and Drug Administration (FDA) and is frequently used for several cancers, including gastric adenocarcinoma, non-small-cell lung cancer, breast cancer, ovarian cancer, and others [4].

In order to cause cell cycle arrest, DTX binds reversibly to microtubules, facilitating the stabilization of trans- sitory structure. Docetaxel is a cytostatic medication as a result, limiting the growth of tumor tissue [5].

Regarding its clinical significance, taxane is crucial in the treatment of metastatic breast cancer. When DTX was compared to other chemotherapeutic drugs, it demonstrated some better metastatic disease survival results [6].

However, due to its poor aqueous solubility (4.93 g/mL in filtered water), high lipophilicity (logP = 4.1), low bioavailability, and significant toxicity, the clinical administration of intravenous DTX has been constrained. To address these pharmacotechnical issues, the pharmaceutical industry created various formulations that include alcohol and/or surfactants like Tween-80 to boost the solubility of DTX. However, because they contain highly reactive ingredients, these formulations can have negative effects on patients, such as fluid retention, neurotoxicity, hypersensitivity, and neurotoxicity of the musculoskeletal system [7].

Researchers are creating several forms of drug delivery systems (DDS), such as nanoparticles (NPs), to lessen these negative effects in order to get around DTX's disadvantages. Solid lipid nanoparticles [8], liposomes [9], nanoemulsions [10], and polymeric micelles [11] are examples of drug delivery systems that may enhance the therapeutic action, stability, and biocompatibility of DTX.

Solid lipid nanoparticles (SLNs) are a desirable DDS among the several types of lipid nanostructures because they have a higher structural stability and biocompatibility than nanoemulsions and are thought to be a less hazardous option to polymer-based nanoparticles [12].

At body and room temperature, SLNs maintain their solid state because they are comprised of physiologically acceptable lipid components [13]. Low toxicity, controlled drug release, physical stability, large-scale production, protection of the drug incorporated, high drug loading, low cost, avoidance of organic solvents in preparation, biodegradability, biocompatibility, and the ability to incorporate hydrophilic and hydrophobic compounds are some benefits of SLNs [14, 15]. As a

result, the invention of docetaxel-loaded SLNs (SLN-DTX) offers a good substitute carrier to lengthen the half-life of docetaxel in the plasma, avoid drug toxicity, and improve docetaxel delivery to tumor tissues [16].

In light of the literature review that was previously mentioned, the purpose of this study was to assess the effectiveness of SLN-DTX both in vitro and in vivo using a tumor xenograft model that was produced in female BALB/C mice.

Results and discussion

One of the most significant chemotherapy medications now on the market is docetaxel. Taxotere, a drug comprising docetaxel and the excipients ethanol and tween 80, is its most used pharmaceutical version. This is a lucrative product with billion-dollar sales, however the medical community feels that the product formulation has to be improved. There is general agreement that ethanol administration should be avoided to minimize the formulation's potential for toxicity. As a result, numerous research institutions are working to develop a commercially viable Docetaxel formulation that could address the shortcomings of the current formulation.

Different kinds of nano-carriers that could be helpful for this proposal were produced by our research team. With an eye toward industrial scale-up, we created a Solid Lipid Nanoparticle for the current paper that could effectively entrap Docetaxel without the need of an organic solvent and that its manufacture was completed entirely in aqueous systems. The SLN created had an encapsulation rate higher than 85%, a finding that is challenging to duplicate in other carrier systems, such as liposomes, and might be considered the pinnacle of our findings.

Additionally, as shown in our findings, this Solid Lipid Nanoparticle performed admirably in terms of tumor management and the avoidance of harmful lung metastasis. Since the investigations were conducted in 4T1 tumor-bearing mice, which have a significant metastatic profile, and we consider a differential result in comparison to other docetaxel nanocarriers, it is extremely crucial to draw attention to this second point.

Preparation, characterization and in vitro release of SLNs

Using high energy, solid lipid nanoparticles were created. Compritol was chosen as the solid lipid, and Span 80 and Pluronic F127 were chosen as the surfactants. The final formulation was determined to be the best formulation that remained stable following the integration of docetaxel based on studies in the literature that informed the selection of this lipid phase [17–19]. In order to reduce the interfacial tension in nanoparticles and prevent their aggregation, it is more beneficial to utilize two surfactants together (in our study, we used Span 80 and Pluronic F127) as opposed to just one [20]. our results in smaller and more stable nanoparticles.

According to a study comparing Pluronic F68 with Pluronic F127, nanoparticles created with the latter material have a better hydrophobic interaction with DTX. This is brought on by Pluronic F127's reduced HLB (hydrophilic-lipophilic balance) value. It produces a superior solution

preparation and may stop the agglomeration of nanoparticles [21]. Therefore, it's crucial to pick the right surfactants for SLN preparations.
The diagram is shown in Figure 1a.

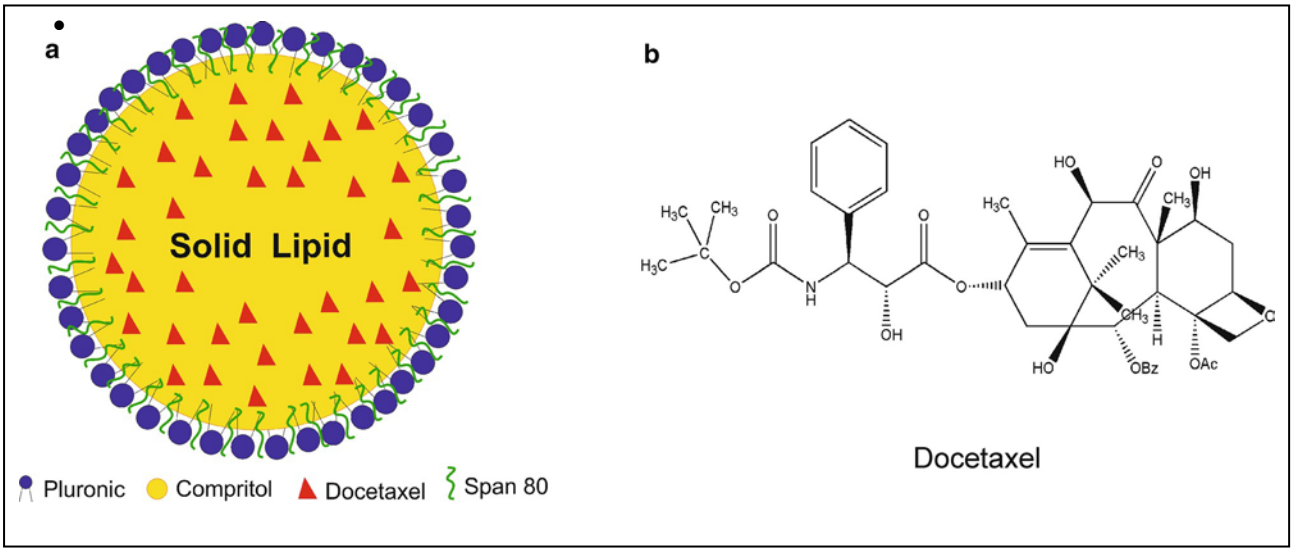

Fig. 1 **a** Schematic illustration of SLN-DTX. **b** Chemical structure of docetaxel (DTX)

Docetaxel-loaded solid nanoparticle model; docetaxel structure is shown in Fig. 1b. Docetaxel's lipophilicity, which in theory would be disseminated throughout the lipid core of the SLNs [14, 22], served as the basis for the model.

The zeta potential parameter measures the charge interaction between the particles and the medium. It is regarded as a starting point for colloidal stability. This parameter aids in the formulation stability by acting as a repelling surface force to keep the dispersed nanoparticles apart [23]. Blank-SLN and SLN-DTX had zeta potential values of 11 and 15 mV, respectively. Zeta potential values between blank and SLN-DTX did not differ significantly, indicating that DTX incorporation did not affect colloidal stability.

Electrostatic attraction is induced by the negative surface charge. It can guarantee the nanoparticles' physical stability while being stored and can stop aggregates from forming [24]. Additionally, negative charged particles have a propensity for having a longer plasma circulation duration [25, 26]. The SLN-DTX has a polydispersity index of 0.153 0.02 and a mean hydrodynamic diameter of 128 2.2 nm. It is crucial to evaluate the colloidal stability of physiological fluids. So, using biological media, we conducted the SLN-DTX interaction (Additional file 1: Figure S1). With the exception of the zeta potential in serum ($p > 0.1$), the DH, PDI, and zeta potential are stable at the sample up to 7 days after simulation.

as a result of corona formation and protein aggregation. Protein adsorption is significantly increased when nanoparticles are added to serum because they come into touch with albumin and other proteins, creating the protein corona. According to some researchers, the formation of protein layers destabilizes nanoparticles, which alters the distribution of surface charges [27].According to studies [28, 29], PDI values less than 0.2 signify a consistent and homogenous dispersion of nanoparticles. Zeta potential, size, and PDI did not change significantly over the course of 120 days, showing that SLN-DTX remained stable (Fig. 2a). The storage stability analysis of SLN-DTX is displayed in Figure 2b. Zeta potential was 15 0.5 mV, PDI was 0.19 0.01, and the average particle size was 126 5.0 nm.

These findings demonstrate the adequate stability of SLN-DTX, with a significant shift occurring only after the fourth particle size measurement (p 0.0001). Samples that underwent this stress test remained stable following a sudden shift in temperature.

The internalization efficiency of spherical, medium-sized nanoparticles with a diameter under 500 nm is improved in the cell. Spherical particles are the ideal shape for attaching to cells and providing a high volume of the medication included [30].

TEM micrographs of blank-SLN and SLN-DTX show that they are uniformly spherical, proving that the presence of DTX would not appreciably alter the shape of the SLNs. The mean particle sizes of SLN-DTX and blank-SLNs are 120 nm and 110 nm, respectively (Fig. 2c).

DLS measures and these outcomes are in agreement.The drug loading and entrapment efficiency of SLN-DTX were 86 2.4% and 2% 0.12%, respectively. The lipid matrix's composition and crystallinity affect the EE% and DL%. According to reports, a crucial factor in the effective encapsulation of pharmaceuticals in lipid-based drug delivery systems is the binding energy of the medications with the lipids [31].The formulation (SLN-DTX) presented similar entrapment efficiency and drug loading comparing to works previously reported in the literature[32, 33].

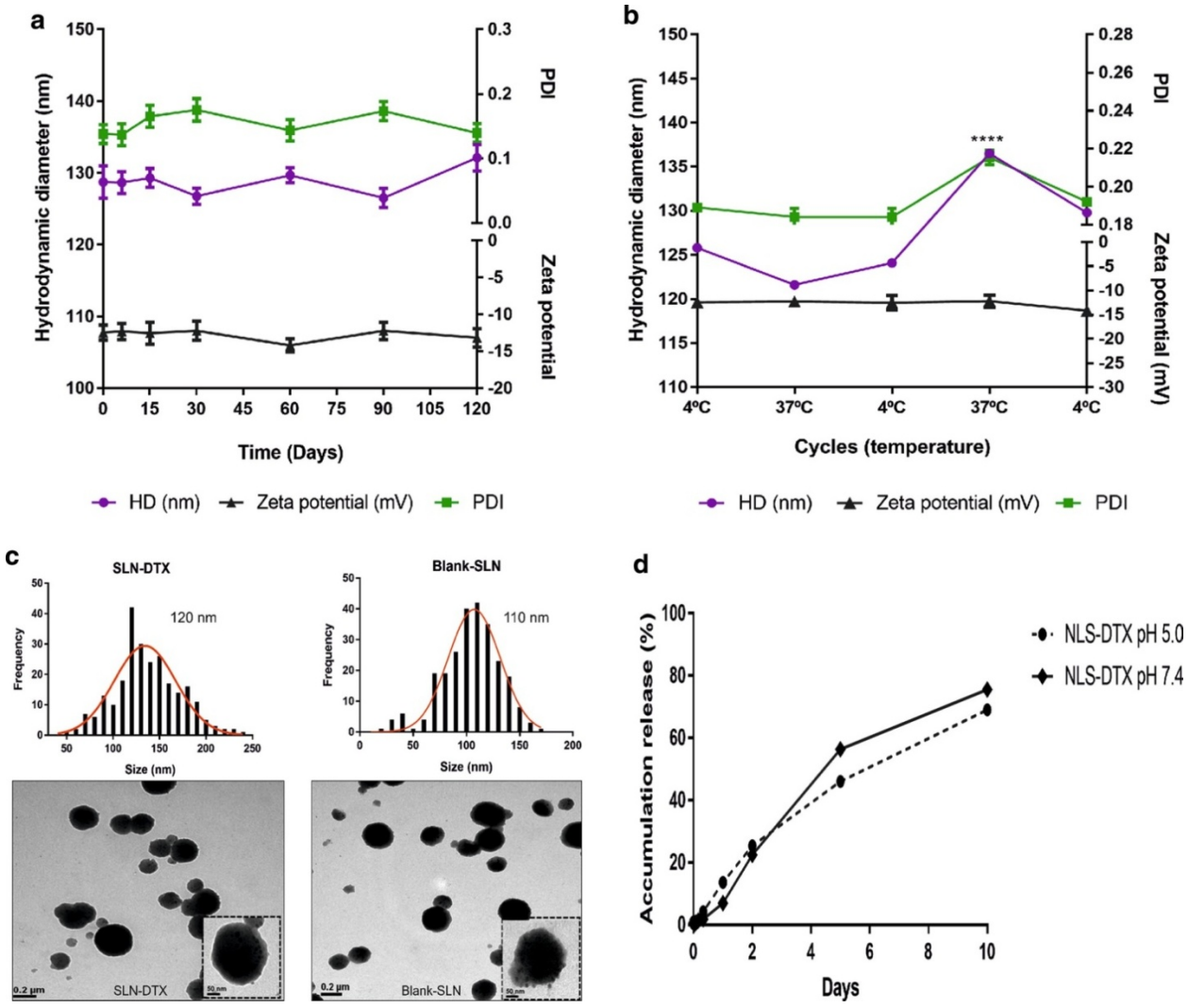

Fig. 2 a Colloidal stability of SLN-DTX over 120 days. Hydrodynamic diameter (HD), zeta potential and polydispersity index (PDI) measured by dynamic light scattering. **b** Storage stability study of SLN-DTX. HD, zeta potential and PDI index were analyzed after samples were incubated for 24 h at 4 °C or 37 °C (n 3). **c** Nanoparticle size distribution of SLN-DTX had an average size of 120 nm and blank-SLN around 110 nm; measurements were performed using ImageJ software. Morphology of SLN-DTX and blank-SLN was assessed by transmission electron microscopy (TEM) at 100 K and in dashed line 250 K magnification. **d** Drug release profiles from SLN-DTX at pH 7.4 and pH 5.0 PBS at 10 days. Data are expressed as mean ± standard error of the mean (****$p < 0.0001$)

At pH levels of 7.4 and 5.0, respectively, to simulate the physiological pH of blood and the acidic intracellular environment of the tumor cells, the in vitro drug release profiles of SLN-DTX

were assessed (Fig. 2d). In SLN-DTX at both pHs, we discovered an initial burst effect release, followed by a controlled release. In 10 days, the percentages of SLN-DTX drug accumulation release reached over 77% at pH 5.0 and 69% at pH 7.4. There were no differences found. The extended release implies uniform DTX trapping throughout the entire system.

This robust interaction could be seen in the FTIR, Raman, and DSC findings. By keeping drug concentrations in a therapeutic window for an extended period of time, the prolonged release method may reduce dose and drug administration [34]. The usefulness of SLNs as a promising medication carrier is confirmed by this profile.

Fourier transform infrared and raman spectroscopy:

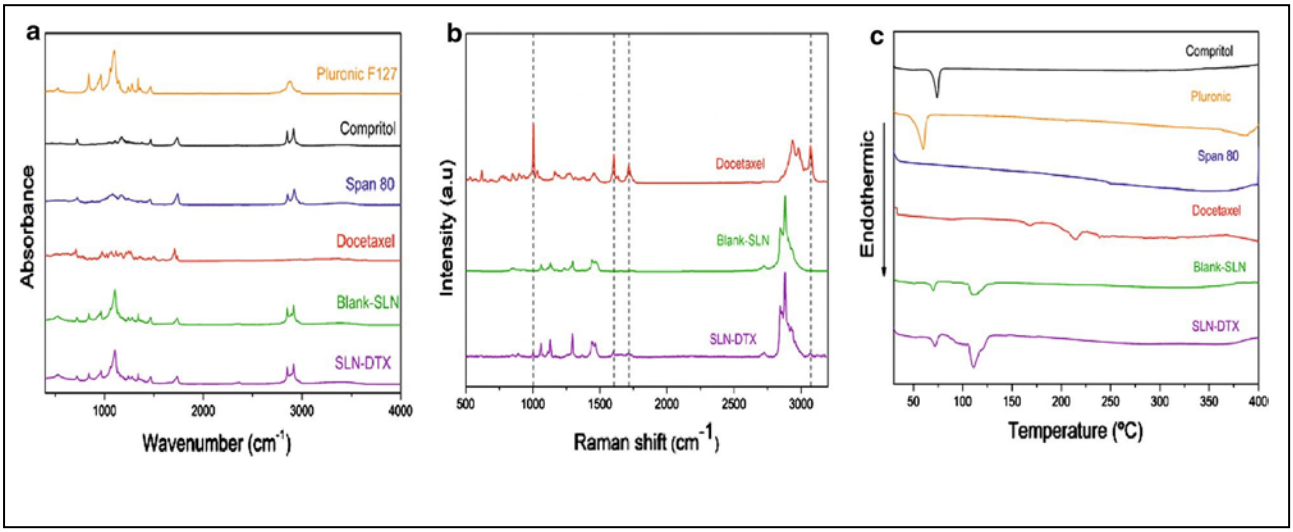

Fig. 3 a Vibrational spectra in the infrared region of Pluronic F127, Compritol, Span 80, docetaxel, Blank-SLN and SLN-DTX. **b** Raman spectra of docetaxel. The highlights represent docetaxel bands in SLN-DTX spectra. **c** DSC thermograms

The interaction level of functional groups in the active substance (docetaxel) with the carrier system was assessed using the spectroscopic approach in the infrared range. The FTIR frequencies and assignments are displayed in Additional file 2: Table S1. Third additional file

Figure S2 displays the DTX FTIR spectrum. The FTIR spectra for the SLN-DTX, blank-SLN, free DTX, and SLN components are shown in Fig. 3-a: Pluronic F127, Compritol, and Span 80. The DTX FTIR spectrum displayed bands at 3369 cm1 (vO-H and N-H), 1437 cm1 (C=C), 2982 cm1 (asCH), 2937 cm1 (sCH), and 709 cm1 (CH), as well as two bands assigned to the vibrational mode C=0, one at 1738 cm1 and one at 1709 cm1, relative to the carbonyl groups of the ester and ketone, respectively [2].

SLN-DTX analysis and Blank-SLN FTIR spectra showed striking similarities. The SLN-DTX FTIR spectra did not show the DTX characteristic bands. Low DTX concentrations in the NLS-DTX make it challenging to identify the bands associated with the drug and evaluate changes in their frequency. As a result, the FTIR approach cannot reliably detect the drug in the carrier. Albano et al. examined similar outcomes. [35]

in a study that used the FTIR technique to detect the lack of the DTX band in lipid-polymeric nanoparticles. There are a variety of physical-chemical interactions that could occur while the nanoparticles are being prepared, such as the creation of hydrogen bonds between the drug and SLN components. This interaction increases the bond stiffness, which changes the vibration frequency [36, 37]. DTX groups may interact with solid lipids. SLNs, on the other hand, exhibit characteristic peaks of related functional groups in their FTIR spectra, confirming the effective creation of nanoparticles without any chemical interaction [38].

Our DTX's Raman spectral signature concurred with earlier observations [39]. (Additional file 4: Figure S3; Additional file 5: Table S2). Figure 3b displays the spectral bands of DTX at 620 and 1006 cm-1, which are attributed to the aromatic vibrations of monosubstituted benzene, and vibrational bands at 1605, 1632, and 1715 cm-1, which were assigned to the ester, aromatic stretch (vC=C), and carbonyl groups, respectively, present in the DTX medication. The presence of the secondary alcohol group is between 1200 and 1430 cm1. Broad bands with shoul- ders in the range of 1200–1500 cm1 are also present and are associated with the deformation of CH2 and CH3 [40].

When compared to the blank-SLN spectra, new bands were visible in the SLN-DTX spectra (Fig. 3b). The presence of these bands indicates the presence of docetaxel. Bands can be seen in the SLN-DTX spectrum at wavelengths of 1006, 1605, 1715, and 3072 cm1. Blank-SLN spectra do not show these bands. The vibrational modes vC=C (aromatic), C=C with C=O, C=O of the carbonyl groups, and (O-H) are attributed to these bands. Even at modest intensities, the existence of these DTX-specific bands allows us to deduce that the drug is present in the lipid system (SLN-DTX).

When the drug was infused into the carrier, it lost some of its crystalline structure as seen by several peaks that were present in DTX spectra decreasing or disappearing in SLN-DTX Raman spectra. The same was observed by Gao et al. [41],Some DTX bands in a study that included

DTX incorporation into albu- min-lipid nanoparticles showed diminished or absent intensity after integration.

Differential scanning calorimetry—(DSC)

In order to learn more about a molecule or formulation's physical and energetic properties, differential scanning calorimetry is typically performed. The DSC technique measures the physical or chemical changes in the material.

Table 1 DSC of solid lipid nanoparticle constituents and docetaxel

Sample	T_{peak}/°C	ΔH (J/g)
Compritol	73.50	95.05
Pluronic	57.51	133.05
Span 80	129	34.60
Docetaxel	168.1	7.92

the amount of heat that samples lose or absorb as a function of temperature [42]. Fig. 3-c displays the thermograms for DTX, Compritol, Plu- ronic F127, Span 80, blank-SLN, and SLN-DTX. Table 1 displays the thermal information (melting point and H) of the SLNs and DTX constituents.

The melting point of the compound in its polymorph form, which is the most stable form, was determined through thermal analysis of Compritol 888 ATO by DSC to be 73.5 °C [17].

Rahman et al.'s research [23] revealed that Compritol 888 ATO's melting point was also 71.2 °C, demonstrating the crystallinity of polymorph. The solid condition of the lipid core within Blank-SLN and SLN-DTX was confirmed by the appearance of the endothermic melt- ing peak of Compritol at 69 to 74 °C. The inclusion of the lipophilic medication and the sustained release features of the lipid nanoparticles depend on the crystalline state of the lipid core [34]. A similar finding was made by Newa et al. [43] and Karolewicz et al. [18] as well. Plu- ronic F127 exhibits an endothermic peak that corresponds to melting at 57.51 °C. Indeed,

The Pluronic F127 endothermic event was recorded by the authors at 57.29 °C and 53.42 °C, respectively. Since Span 80 is a liquid at ambient temperature (the first analysis temperature), it is impossible to see its melting point using DSC. At 129 °C, Span 80 deterioration first occurs [19].

The endothermic peak in the DSC curve of DTX, which corresponds to the drug's melting point, is seen at 168.1 °C [44]. In the DSC thermogram of SLN-DTX, this endothermic peak of DTX

was no longer visible. The transformation of originally crystalline DTX into an amorphous state or disordered lipid core would indicate the occurrence of strong drug-lipid interactions [8, 45].

It has been demonstrated in the past that the loss of DTX crystallinity is correlated with the lack of the distinctive DTX peaks in DSC [8, 46]. Polymeric particles containing DTX were examined by Sanna et al. [47] for the treatment of prostate cancer. The authors noticed that the DTX melting peak totally vanished from the DSC curve in all of the nanoparticle samples they examined, proving that there was no crystalline drug present. Data from other earlier research also demonstrate that it is not possible to see DTX fusion-related peaks in the DSC curve of the drug-containing nanoparticle simulation [7, 45, 48-50].

Furthermore, the robust DTX-lipid association may also be to blame for the slower release of DTX from SLN-DTX, as demonstrated by the in vitro study's findings.

In vitro cytotoxicity studies—MTT assay:

The MTT experiment was carried out using breast cancer cell lines (4T1 and MCF7) and non-cancerous cells (NIH-3T3 and HNTMCs) to assess the cytotoxicity of SLN-DTX and free DTX. To rule out any effects that were not specifically targeted, the results were compared to those of a therapeutically accessible DTX formulation. For 24 hours (Figs. 4 and 5a, c) and 48 hours (Figs. 4 and 5b, d), cells were exposed to concentrations of 0.001, 0.01, 0.1, 1, 10, and 100 g/mL equivalent DTX. Blank-SLN produced results that were comparable to those of untreated cells and had no impact on the viability of the cells. The blank-SLN formulation can be used for intracellular applications because it is biocompatible and suited for that purpose.

The IC50 values for free DTX against 4T1 cells were 10 g/mL (24 h) and 0.3 g/mL (48 h), suggesting time- and dose-dependent cytotoxicity (Fig. 4a, b). The IC50 values for SLN-DTX against 4T1 cells were 0.08 g/mL (24 h) and 0.01 g/mL (48 h). IC50 values for SLN-DTX were 1.04 g/mL (24 h) and 0.05 g/mL (48 h), and for free DTX were 12.19 g/mL (24 h) and 10.01 g/mL (48 h), according to data from MCF7 cells (Fig. 5a, b). In contrast to free DTX, which was hazardous to both human and murine non-cancerous cells (HNTMCs and NIH-3T3), SLN-DTX demonstrated greater cytotoxicity against cancer cells.

After 24 hours of treatment, SLN-DTX showed a considerably lower IC50 value (p 0.0001) and a concentration that was more than 100 times lower than free DTX, showing higher cytotoxicity and efficiency of nanoparticles. According to the release study, it was determined that the SLN-DTX was more effective because it released less drug (69.4 g/mL) over the course of 24 hours compared to free DTX, which released 1000 g/mL at the same time and had comparable cytotoxic effects. These findings are in line with earlier research that demonstrated that drug-loaded lipid-based nanoparticles had a higher cytotoxicity than free medications [4, 34, 47, 51, 52].

According to our TEM (internalization) and uptake results, the improved efficacy mechanism of SLN-DTX cytotoxicity may be caused by its quick absorption and high permeability, which allow the intracellular nanoparticles to accumulate and be mediated via endocytosis [2, 16].

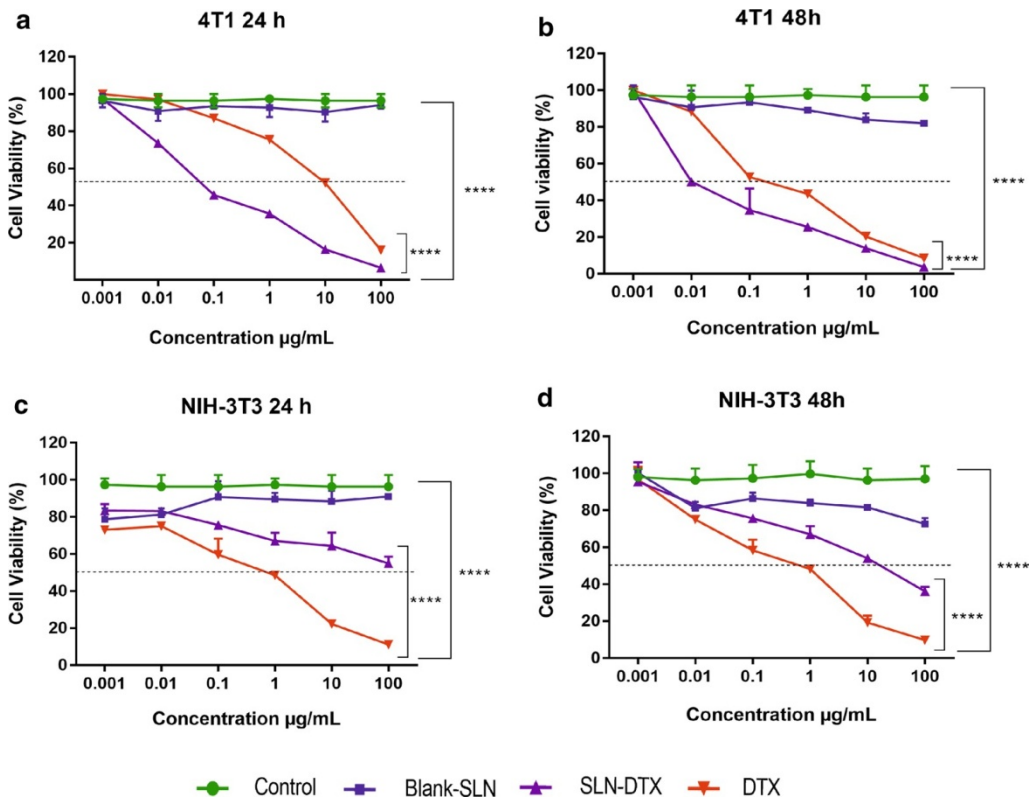

Fig. 4 Viability of 4T1 (**a**, **b**) and NIH-3T3 (**c**, **d**) cells after 24 and 48 h treated with free DTX, blank-SLN and SLN-DTX at 0.001, 0.01, 0.1, 1, 10 and 100 µg/mL (equivalent DTX concentrations), evaluated by MTT assay. Data are expressed as mean ± standard error of the mean (****$p < 0.0001$)

4T1 morphology:

Phase contrast and scanning electron microscopy observations demonstrated the morphological differences between the treated and untreated cells. Both of the methodologies utilized allowed for these changes to be seen (Fig. 6). The majority of the control cells had the expected typical cytoplasmic projections and a smooth cellular surface (Fig. 6a). Both cells' shapes changed as a result of DTX and SLN-DTX exposure, and their cytoplasmic projections shrank. Similar

findings from earlier research have been reported [53, 54]. These morphological surface changes might be connected to the DTX-induced disturbance of cytoskeleton dynamics [55]. The DTX-induced impairment in microtubule remodeling can have an impact on the shape of the cell surface.

Cell cycle analysis and cell apoptosis

One of the traits of cancer cells is the dysregulation of the cell cycle. Therefore, to stop the development of abnormal cancer cells, cell cycle arrest may be a suitable and useful technique [56]. It has been demonstrated that docetaxel causes microtubule damage, prolonging the G2-M arrest and leading to apoptosis [57]. Fig. 7-a displays the cell cycle analysis of 4T1 cells subjected to SLN-DTX or DTX. In line with earlier findings [57–59],

cells treated with SLN-DTX or DTX saw a substantial drop in G0/G1 phase compared to control cells, causing an arrest in the G2-M phase. In cells treated, the accumulation in the G2-M phase was noticeably higher ,DTX was released into the cytosol, causing cell cycle arrest in the G2-M phase, as seen by the higher percentage of cells treated with SLN-DTX (73.7) compared to cells treated with free DTX (67.8%). These findings support the data acquired from MTT analysis and offer more proof of the possible clinical uses of SLN-DTX.

The primary cell death mechanism in response to taxanes is thought to be apoptosis. Phosphatidylserine, a lipid that can be marked with fluorochrome-conjugated annexin V, is present on the inner surface of the cell membrane and is externalized by cells during apoptosis. Propidium iodide (PI) often does not interact with living cells that have intact membranes, whereas the membranes of dead cells are permeable to PI [60].

It is feasible to distinguish between healthy cells, which stain negatively for annexin V-FITC and propidium iodide, early apoptosis, which stain positively for annexin V-FITC but negatively for PI, late apoptosis, which stain positively for both annexin V-FITC and PI, and necrosis, which stain positively for PI [59]. Nuclear cytoplasmic condensation and chromatin aggregation are two morphological and biochemical alterations that characterize apoptotic cells. Necrosis, on the other hand, demonstrates a passive response to severe cellular damage and has physiological effects that are significantly different from those of apoptosis. The cell's capacity to maintain homeostasis is compromised in necrosis [61].

The cells collecting in the lower right quadrant of the dot plot between Annexin V-FITC and propidium iodide represent early apoptosis. The early and late apoptotic rates in the control group were 5.5% and 1.5%, respectively, as shown in Fig. 7b. Early apoptotic cells in the presence of SLN-DTX displayed a rate of 82.5% as opposed to the free DTX's 67.8%, which could be due to the increased availability of DTX in SLNs. These findings support the data from cell cycle analysis and indicate that, in comparison to DTX, SLN-DTX considerably improved DTX-dependent apoptosis in 4T1 cells.

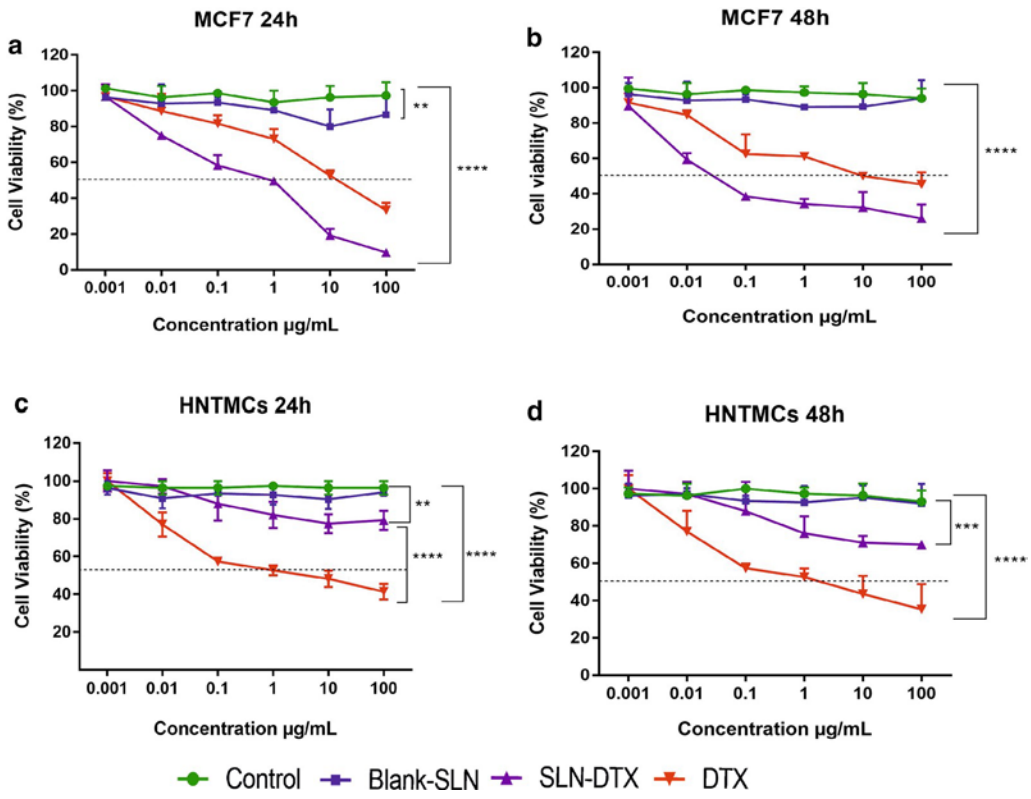

Fig. 5 Viability of MCF7 (**a**, **b**) and HNTMCs (**c**, **d**) cells after 24 and 48 h treated with free DTX, blank-SLN and SLN-DTX at 0.001, 0.01, 0.1, 1, 10 and 100 µg/mL (equivalent DTX concentrations), evaluated by MTT assay. Data are expressed as mean ± standard error of the mean (**p < 0.01; ***p < 0.001; ****p < 0.0001)

Effects of DTX on microtubules in 4T1 cells

By attaching to the tubulin subunit, DTX can produce a cytotoxic impact [62]. Untreated cells are depicted in Fig. 8 as having vast, well-defined, and structured microtubule networks. On the other hand, cells treated with free DTX and SLN-DTX displayed stabilized, shorter, and straighter microtubules, resulting in elongated bundles of microtubules that curled around the cytoplasm, indicating a shift in the regulation of microtubule dynamics from DTX.

Internalization of SLN-DTX by TEM and analysis of cellular uptake

The features of the cellular ultrastructure and SLN-DTX uptake were confirmed using TEM. To improve the effectiveness of chemotherapeutics, pharmacological carriers based on lipids, such as SLNs, have been employed extensively [63]. Previous research has shown that different cell types internalize lipid nanoparticles via the endocytic route [63, 64]. According to the method of internalization, the internalized nanoparticles were predominantly concentrated in the cytoplasm

of the cell's lysosomes and/or endosomes (Fig. 9a III-VI). It appears that some of the nanoparticles are being broken down inside the vesicles. Nanoparticles appear to be grouped in clusters, although they can still be distinguished as individual particles (Fig. 9a III-VI). It is possible to see the nucleus, and the photos repeatedly show that SLN-DTX was not present there (Fig. 9a III). Figure 9a I–II shows the control cells.

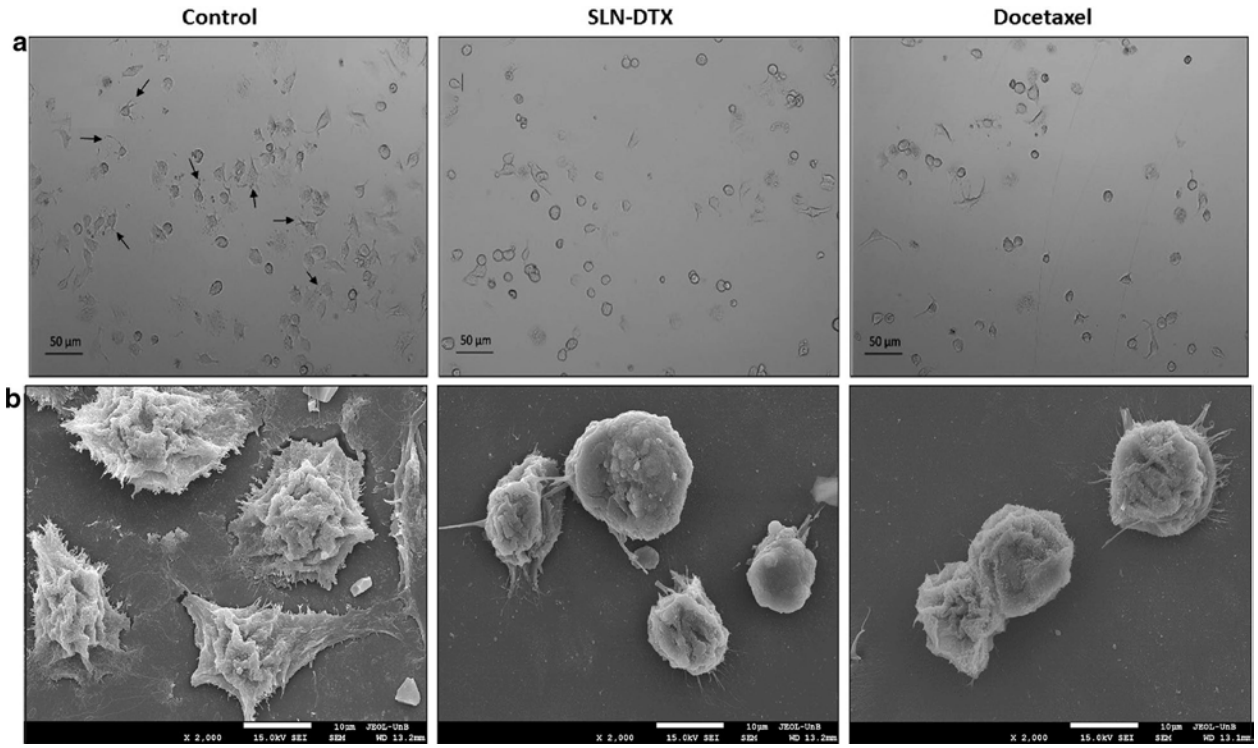

Fig. 6 Morphology of murine breast adenocarcinoma cells (4T1). **a** Light microscopy (phase contrast). **b** Scanning electron micrograph (SEM). Control cells (without treatment), cells treated with SLN-DTX or DTX. The arrows show the cytoplasmic projection in cells. Cells were treated at 10 µg/mL for 24 h. Objective: 10×. The micrographs (SEM) were performed at 2 k

The intracellular accumulation of DTX was examined in 4T1 cells using an HPLC technique to gauge cellular absorption effectiveness. Comparing cellular absorption of SLN-DTX with free DTX was done. The results demonstrated that at times of 4 hours, 18 hours, and 24 hours, SLN-DTX absorption by the cell was significantly higher than for free DTX. In cells treated with SLN-DTX, the DTX uptake accumulation is time-dependent and grows with time. In contrast, cells fed with free DTX accumulate DTX for 4 hours before the concentration decays (Fig. 9b). When compared to free TXT, Mosallaei et al. [8] shown that TXT from the absorption of solid lipid nanoparticles in C-26 cells is larger. These results imply that the use of SLN-DTX may allow DTX doses to be decreased without losing therapeutic benefit, decreasing the toxicity of the medication.

In vivo antitumor efficacy:

Five doses of 10 mg/kg DTX each were administered to 4T1 tumor-bearing Balb/c mice to compare the in vivo therapeutic efficacies of free DTX and SLN-DTX. The dose was chosen in consideration of earlier literary works (4,44,65). The group receiving SLN-DTX demonstrated the lowest tumor growth rate, which was consistent with the data on invitro cytotoxicity (Fig. 10a). Tumor volume data revealed that while those in the PBS and Blank-SLN groups in mice developed quickly, those in the docetaxel and SLN-DTX groups grew more slowly. At the end of the study, docetaxel treatments and SLN-DTX treatments both dramatically reduced tumor growth compared to the PBS group, with docetaxel inhibiting tumor development by roughly 42.7% and 92.7%, respectively.

Our findings were supported by a prior study [16] that demonstrated tumor regression in mice treated with encapsulated DTX (10 mg/kg) was more effective than free DTX.

The analysis revealed no statistically significant difference in mouse weight between the groups, demonstrating the low systemic toxicity of various treatments at the prescribed dose (Fig. 10b). The hematological and biochemical parameters did not alter significantly either (Additional file 6: Table S3).

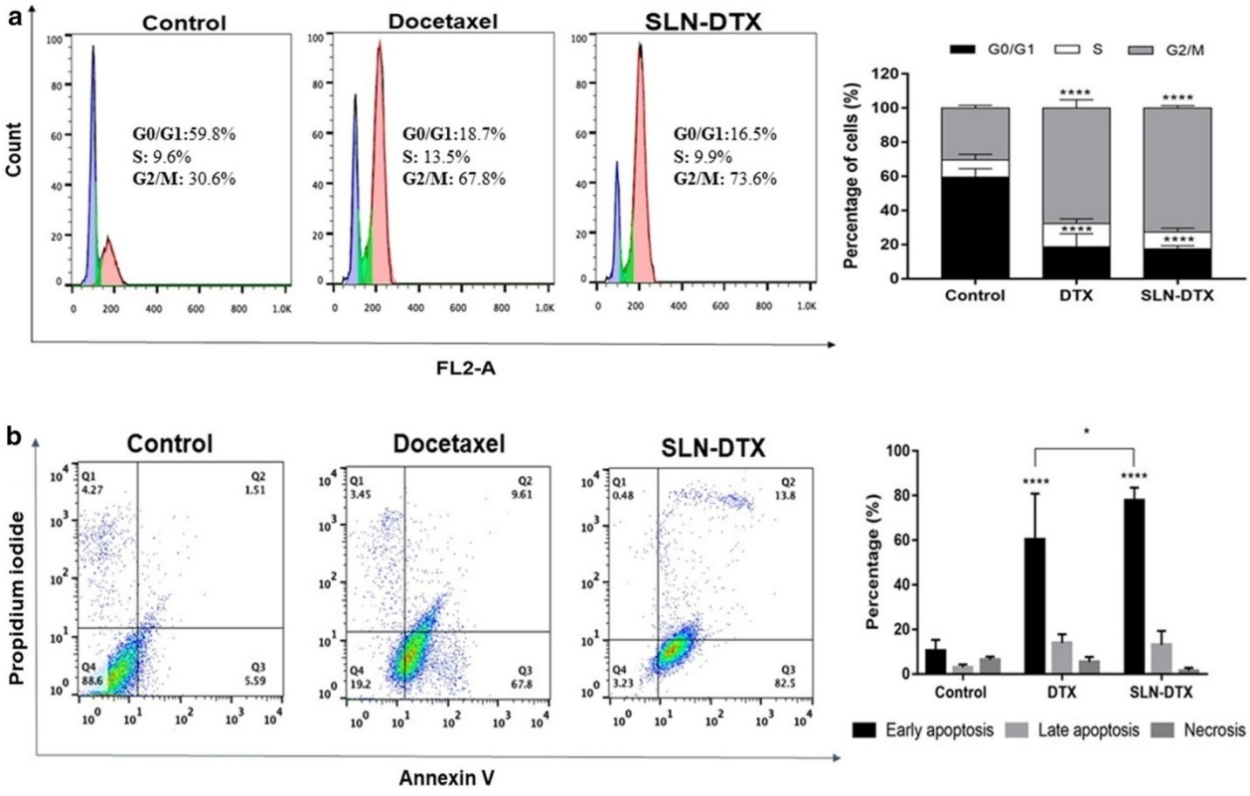

Figure 7a shows representative flow cytometry profiles of the distribution of 4T1 cells' cell cycle phases. The first peak (purple) signifies 2n DNA content in the G0/G1 phase, the second peak (pink) suggests 4n DNA content in the G2/M phase, and the S phase (green) is located in between the two peaks. b Dot plots showing the location of apoptotic cells following dual labeling with propidium iodide (vertical axis) and annexin V-FITC (horizontal axis). Propidium iodide and annexin V-FITC-tagged cells represent early and late apoptosis, respectively (lower right

quadrant and upper right quadrant). The percentage of the cells is shown on the right side. groups: SLNDTX, DTX, and untreated cells. 10 g/mL was applied to the cells for 24 hours.Data are presented as mean ± standard error from three experiments (*$p < 0.05$; ****$p < 0.0001$)

Lung metastasis prevention and IL-6 serum level of 4T1breast cancer

We looked at how SLN-DTX medication could stop lung metastasis that develops on its own. Spontaneous metastasis typically happens in advanced stages of disease, and 4T1 breast cancer metastasis mostly affects the lungs and shares many traits with human breast cancer [66].

We could plainly identify several metastatic nodules around the lungs in the PBS and Blank-SLN groups (Fig. 11a). Metastatic nodules were slightly lessened after DTX therapy. The absence of metastasis in the SLN-DTX group suggests that this drug can significantly limit the metastasis of 4T1 breast cancer to the lung while also reducing the number of tumor nodules and their size (Fig. 11b).

H&E staining analysis was used to further confirm the metastasis. According to Fig. 11c, there were several tumor metastasis loci (red dotted circle) found in the lungs of the PBS and Blank-SLN groups, a moderate number in the lungs of the docetaxel group, and none in the lungs of the SLN-DTX group. These findings imply that SLN-DTX outperforms free docetaxel in its capacity to prevent tumor spread to the lungs.

Unbalanced cell proliferation is linked to the development of tumors, immune system evasion, and the potential for metastasis. These alterations are connected to a change in cytokine production [67]. A pleiotropic cytokine called interleukin-6 (IL-6) controls pro-inflammatory and metastatic tumor growth. According to studies, people with breast cancer have higher amounts of IL-6 in their blood. High IL-6 levels are linked to the onset, progression, and metastasis of cancer [67, 68].

Additionally, a prior study found that mice with breast tumors that expressed high levels of IL-6 spontaneously developed liver and lung metastases [69]. As a result, we measured the serum levels of IL-6 in mice following treatments.

In our findings, IL-6 levels were significantly higher in the PBS, Blank-SLN, and DTX groups than in the healthy control group, indicating the presence of metastatic disease in the lungs (as demonstrated by H&E and lung metastasis results). These groups had IL-6 levels of 628 3.4, 568 1, and 345 6.6 pg/mL, respectively. The healthy control group and the SLN-DTX treated group did not differ significantly from one another (Fig. 11d).

These results confirm the critical contribution of IL-6 levels to invasion and metastasis of breast cancer. High IL-6 serum levels have been demonstrated in studies by Salgado et al. [67] to be

associated with a worse survival rate in patients with advanced breast cancer, and at later stages, high levels may stimulate tumor development.

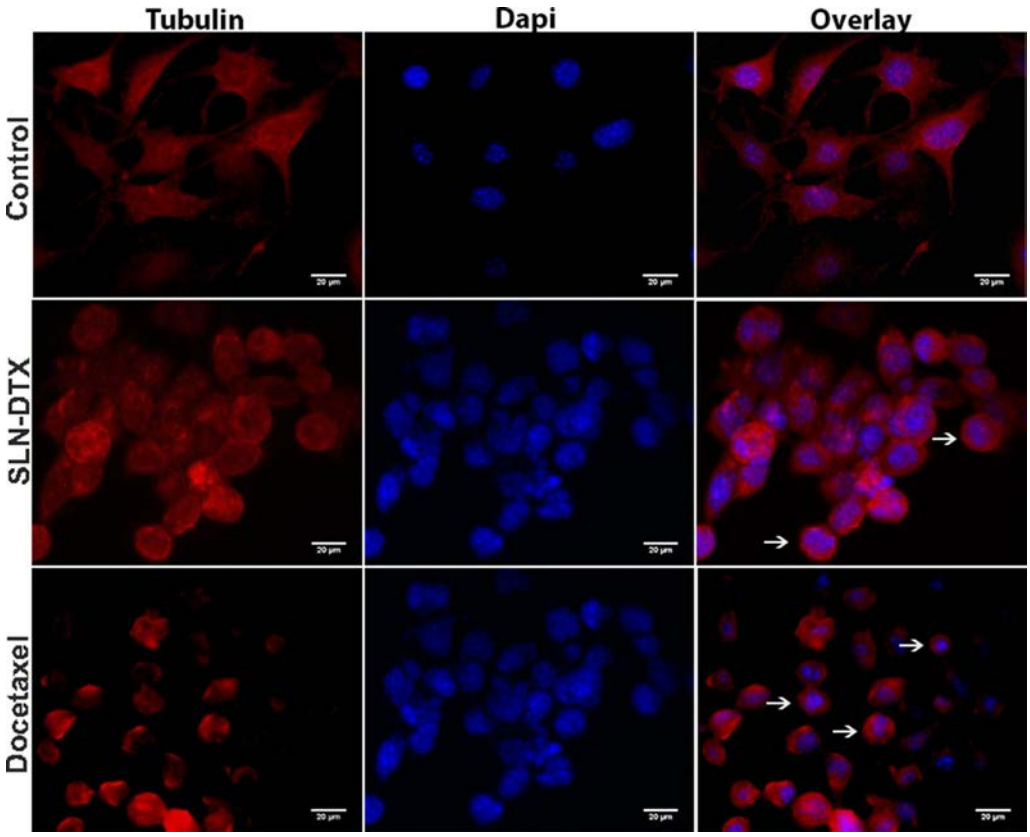

Fig. 8 shows a 4T1 cell immunofluorescence experiment. For 4T1 cells that were left untreated or treated with SLN-DTX or DTX 10 g/mL for 24 h, microtubules and nuclear staining are shown separately (Tubulin and DAPI, respectively) and together (Overlay). Microtubule bundling is depicted by the arrows. (Objective 63 x)

Bcl-2 and Ki-67 immunohistochemistry analysis

A proto-oncogene associated with apoptosis and programmed cell death is Bcl-2. Overexpression of the Bcl-2 protein has been linked to an increase in breast cancer invasion and migration, according to studies [70, 71]. We looked into Bcl-2 in lung and tumor tissues using immunohistochemistry in this context, based on findings about metastasis prevention by SLN-DTX treatment (Fig. 12). When compared to the SLN-DTX group, which revealed statistically significant differences (Fig. 12c, f) (p 0.0001), strong Bcl-2 staining was seen in the groups previously identified with lung metastasis, i.e. the PBS, Blank-SLN, and DTX groups.

In order to assess cell proliferation in the tumors and lungs following treatments and control groups, we used the Ki-67 assay. The research showed that the PBS, Blank-SLN, and DTX

groups all had strong positive indices. In comparison to the PBS control group, the SLN-DTX treatment generates significantly decreased (p 0.0001) levels of cellular proliferation (Fig. 12b, e). These findings therefore indicated that, as previously noted, SLN-DTX is related with the suppression of tumor growth and induces a decrease in cell proliferation.

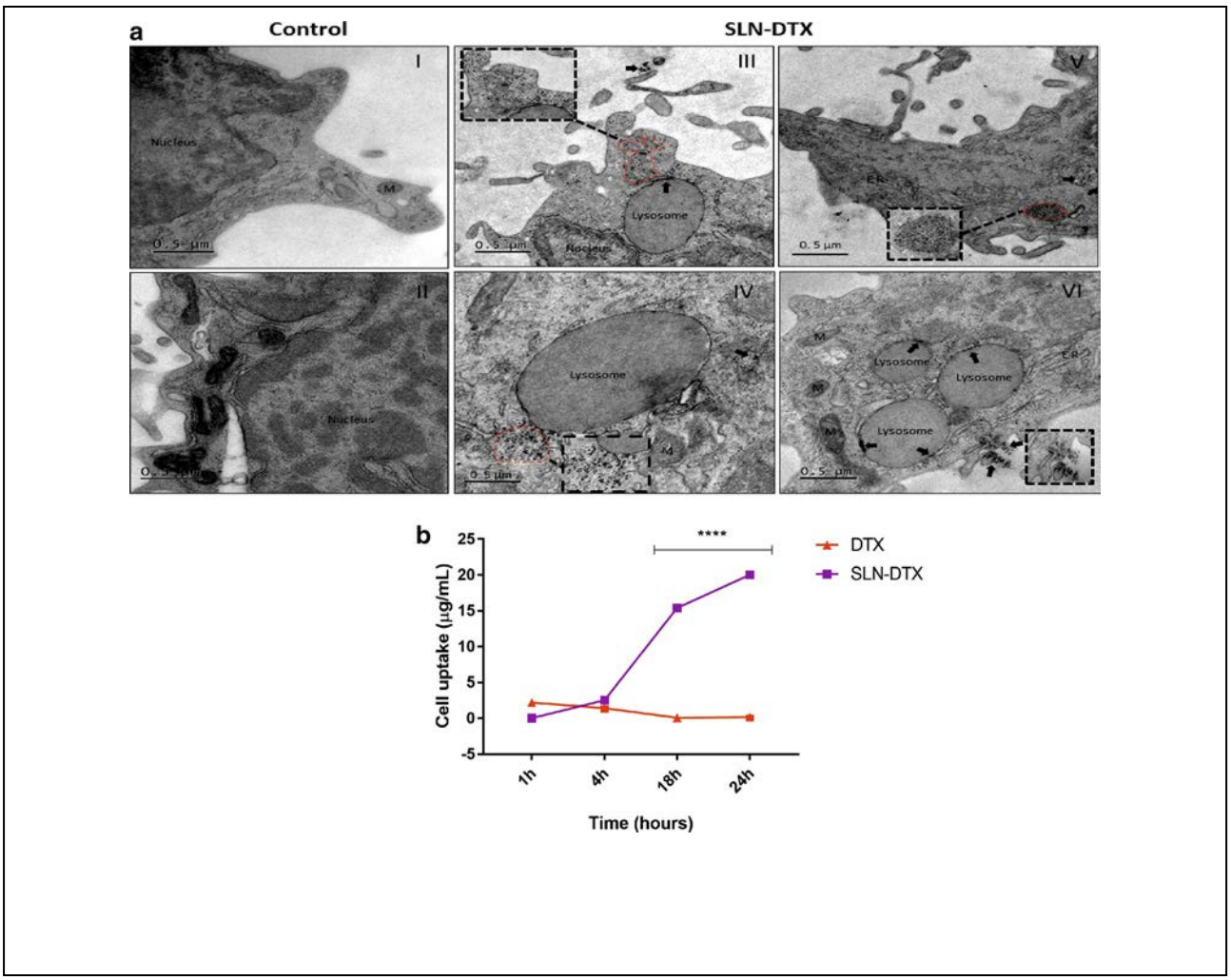

Ultrastructural photos of 4T1 cells are shown in Fig. 9. (I-II) Untreated control cells. (III-VI) Cells that were exposed for 24 hours to 10 g/mL of SLN-DTX. Internalization of SLN-DTX is shown in (III-V) by dashed lines; internalization of SLN-DTX into lysosomes is shown in (VI) by arrows. Nanoparticles are denoted by dashed lines, arrows (into lysosomes), and arrow heads. the mitochondria, and ER the endoplasmic reticulum. Magnification (black dashed lines): 5 K; 15 K. b Research on the in vitro uptake of DTX by 4T1 cells. Cells were treated to SLN-DTX or DTX at concentrations of 100 g/mL for 1, 4, 18, and 24 hours. The mean and standard error of the mean are how data are presented (****p 0.0001).

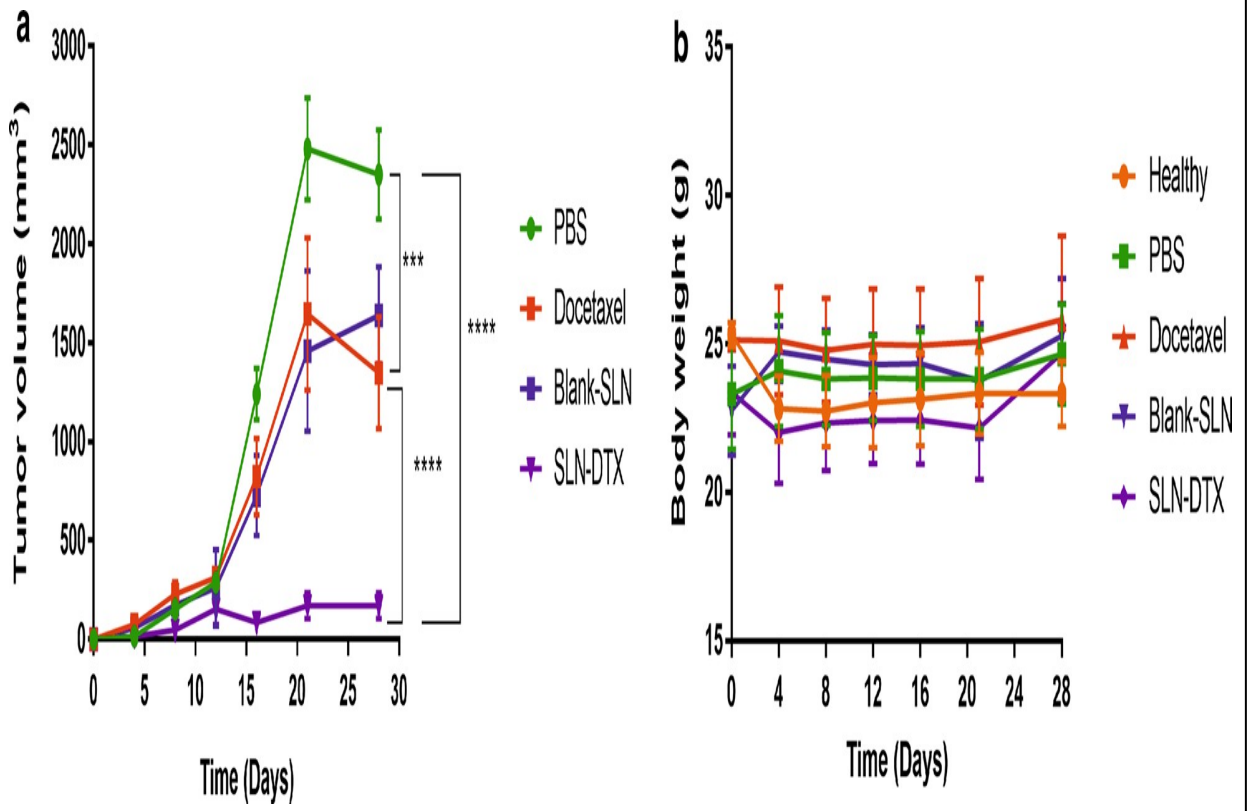

Fig. 10 Antitumoral effect of SLN-DTX, Docetaxel, Blank-SLN and PBS on 4T1 tumor-bearing Balb/c mice. **a** Variation of tumor volume and **b** mice weight. ***$p < 0.001$; ****$p < 0.0001$, compared with PBS group

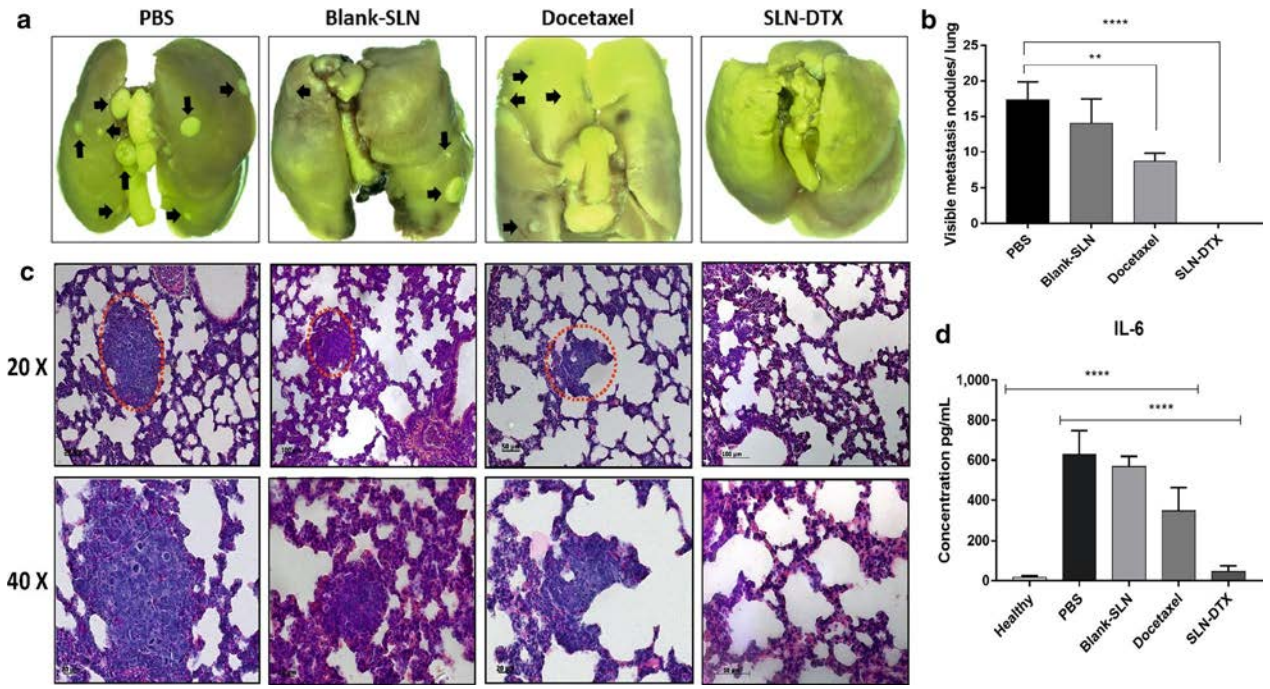

Fig. 11 **a** Photo of lung. **b** Statistical analysis of numbers of tumor nodules on the lungs. **c** Histopathological examination of the lungs. **d** IL-6 serum levels of mice were measured by ELISA. The metastasis was marked by red dotted circle and black arrows. Data represent mean values ± standard error (**$p < 0.01$; ****$p < 0.0001$)

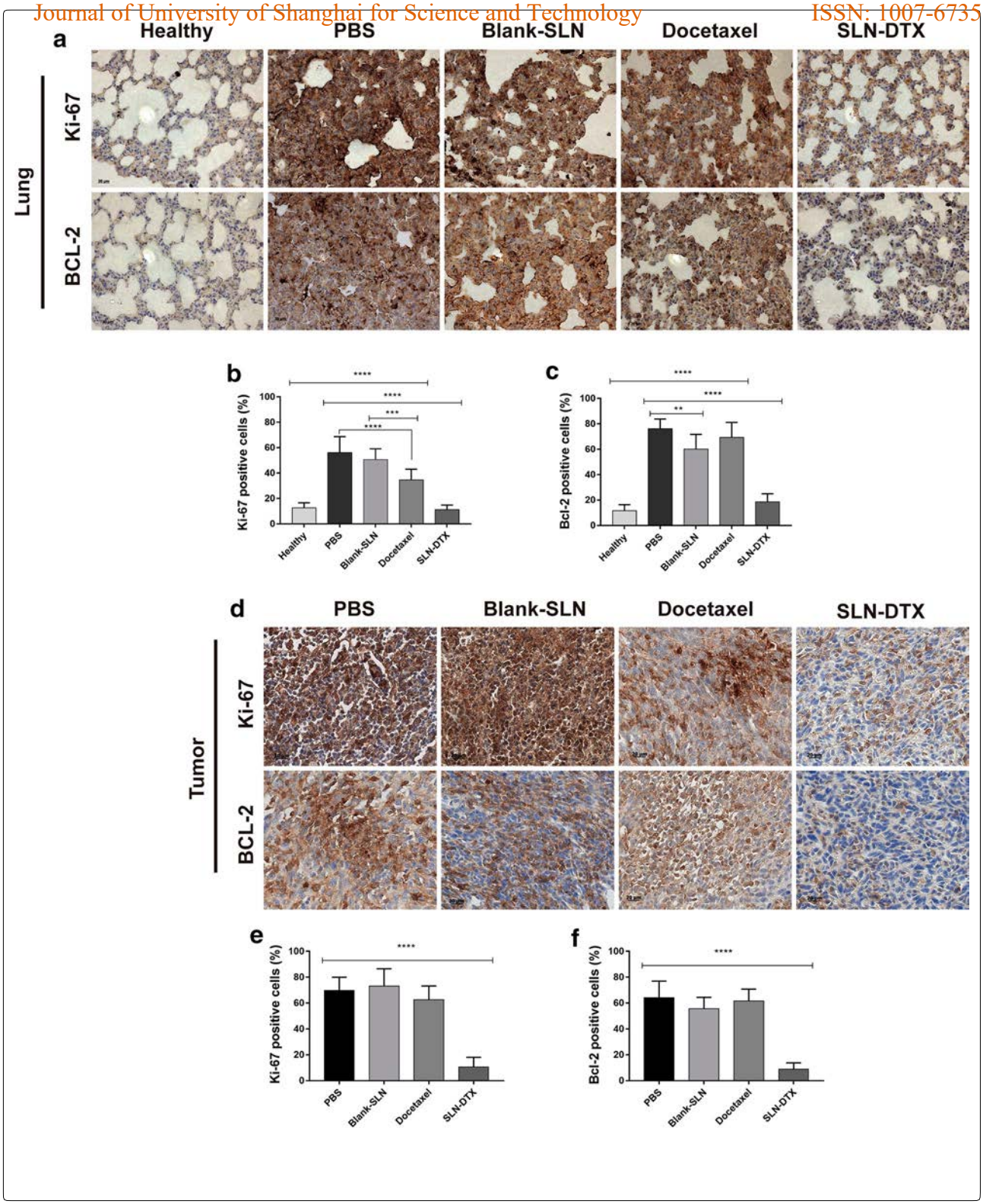

Fig. 12 Immunohistochemistry analysis. The brown dye-stained cells represent positive cells. **a** Lung and **d** tumor slides were immunostained with anti-Ki-67 and BCL-2. **b**, **e** Quantification of Ki-67 and **c**, **f** BCL-2 staining. Data represent mean values standard error (**p < 0.01; ***p < 0.001;****p < 0.0001)

Conclusions:

The high-energy technique was used to successfully prepare SLN-DTX. The findings shown that SLN-DTX has excellent encapsulation efficiency (86%), is uniformly distributed, and is stable over time. A sustained and continuous release pattern of SLN-DTX was observed in the in vitro release research. DSC verified that the DTX in SLN-DTX was amorphous. The in vitro experiments showed that SLN-DTX has greater tumor cell cytotoxicity, effective cellular uptake, and cell cycle progression arrest in the G2/M stage. It also caused more apoptosis in 4T1 cells at a lower dose than DTX. Through an endocytosis process, SLN-DTX was taken up by the 4T1 cells and primarily found in the lysosomes. In vivo research showed that SLN-DTX, at a dose of 10 mg/kg, not only dramatically slowed the progression of 4T1 breast cancer tumors, but also prevented lung metastasis without manifesting systemic toxicity in mice. Our research suggests that SLN-DTX suppresses tumor development and prevents lung metastasis by lowering serum IL-6 production, increasing tumor cell death, reducing tumor cell proliferation, and down-regulating BCL-2 expression. These findings support the hypothesis that SLN-DTX is a viable alternative and potentially biocompatible formulation for the treatment of breast cancer.

Materials

The following items were bought from Sigma: Docetaxel, MTT, Annexin, Propidium iodide, Pluronic F127, Span 80, and Compritol ATO 888. The Rio de Janeiro Cell Bank provided the mouse mammary cell line (4T1), human breast cancer cells (MCF7), and mouse embryo fibroblast cell line (NIH-3T3). Fetal bovine serum (FBS), Roswell Park Memorial Institute medium 1640 (RPMI), Dulbecco's modified Eagle's medium (DMEM), penicillin, and streptomycin were purchased from Gibco, Invitrogen. Thermo Fisher provided the MTT (3-[4,5-dimethylthiazol-2-yl]-2,5 diphenyltetrazolium-bromide), Electron Microscopy Sciences in Hatfield, Pennsylvania provided the osmium tetroxide, and J.T. Backer provided the acetonitrile (99.95%—grade HPLC). Other compounds were all of the analytical variety.

Methods

Preparation of solid lipid nanoparticles (SLNs):

By using high energy, blank-SLN (SLN without docetaxel) or SLN-DTX were pre-pared. In a nutshell, the oil and aqueous phases were made separately. After melting and maintaining the oil phase at 80 °C, Compritol (500 mg), Span 80 (50 mg), and Pluronic F127 (450 mg) were added. The oil phase was then heated with DTX (20 mg) until it melted completely. At the same temperature (80 °C), the oil phase was introduced dropwise to the aqueous phase (20 mL of PBS), which was then continuously stirred at a high speed for 10 minutes with an Ultra-Turrax T25 (IKA Werke, Saufen, Germany) at 10,000 rpm. The products have been distributed in PBS, which is their ultimate state.

Determination of hydrodynamic diameter (HD),polydispersity index (PDI) and zeta potential

Dynamic light scattering (DLS) was used at 25 °C to measure the physicochemical characteristics of SLN-DTX throughout the course of 120 days, including hydrodynamic diameter, PDI, and zeta potential. After dilution (1:20) with distilled water, all measurements were performed.SLN-DTX was kept at 4 °C for 24 hours to evaluate the storage stability before being removed and subjected to DLS analysis for mean hydrodynamic diameter, PDI, and zeta potential. The same sample was then kept at 37 °C for another 24 hours while the measurement was carried out, and so on until a total of 5 readings had been made.After each cycle, the same variables were assessed.Samples were diluted (1:20) in distilled water, PBS, cell medium (10% v/v in PBS), and serum (10% v/v in PBS) to study how SLN-DTX interacted with biological media. Up to 7 days following formulation, hydrodynamic diameter, PDI, and zeta potential were recorded using DLS.

Transmission electron microscopy

Using a transmission electron microscope (TEM; JEOL 1011, Tokyo, Japan) run at an accelerating voltage of 100 kV, the size and morphology of SLN-DTX were characterized. After depositing a drop of the sample (5 L) on a copper grid coated with Formvar film that has a 400-mesh mesh, the samples were air-dried and contrasted with osmium tetroxide vapor. Until analysis, grids were stored at room temperature. Image J software was used to measure a minimum of 400 particles.

Quantification of DTX by high performance liquidchromatography (HPLC)

HPLC was used to measure the DTX concentration (Shimadzu, Kyoto, Japan). The stationary phase was made up of a precolumn (1 0.4 cm, 5 m particle diameter) and a reversed phase ACE AQ C18 column (25 0.4 cm, 5 m particle diameter) from ACE Aberdeen, Scotland. The temperature of the column was kept constant at room temperature. Acetonitrile and deionized water made up the mobile phase (55:45, v/v).

At a pressure of 120 kgf/cm2, the injection volume was 20 L, and the flow rate was 1 mL/min. Throughout each run, the column's temperature was kept at 30 °C. The wavelength used for UV detection was 232 nm. A calibration curve was created using DTX doses ranging from 0.01 to 1 mg/mL (y = 21752x 128538, R2 = 0.9994).

In vitro drug release study:

The dialysis bag (14 kDa Sigma, USA) method was used to determine the drug release behavior from SLN-DTX. The releasing medium was Phosphate-Buffer Saline (PBS, pH 7.4 or pH 5.0),

with 0.1% Tween-80. 50 mL of release media were added to the bag holding the SLN-DTX (1 mg/mL of DTX), which was then incubated at 37 0.5 °C with 100 rpm of horizontal shaking. At predetermined intervals (0, 0.25, 0.5, 1, 2, 4, 6, 48, 72, 120, and 240 h), samples were taken out and immediately replaced with the same volume of fresh release medium. HPLC was used to determine the released DTX content**.**

Determination of encapsulation efficiency and drug loading of SLN-DTX

In order to facilitate the separation of the DTX from the other lipid components, SLN-DTX (formulation dispersed in PBS) was centrifuged at 3000 rpm for 10 min. The supernatant was then collected, diluted 1:10 (v/v) in DMSO, and subjected to an ultrasonic bath for 5 min. To quantify DTX using high performance liquid chromatography (HPLC), this mixture was first diluted (1:100, v/v) in the mobile phase, which was made up of acetonitrile and deionized water in a ratio of 55:45 (v/v). This mixture was then gently centrifuged at 2500 rpm for 5 minutes to aid in the sedimentation of remaining lipids. Drug loading (DL%) and entrapment efficiency (EE%) were computed as follows:

$$\text{Entrapment efficiency (EE\%)} = \frac{\text{weight of DTX in SLNs}}{\text{weight of DTX used in SLNs preparation}} \times 100 \quad (1)$$

$$\text{Drug loading (DL\%)} = \frac{\text{weight of DTX in SLNs}}{\text{Weight of SLNs}} \times 100 \quad (2)$$

Fourier transform infrared spectroscopy (FTIR)

Fourier transform-infrared spectroscopy (Vertex 70, Bruker, Billerica, USA) was used to observe the changes within the functional groups of the samples. By using the ATR (attenuated total reflectance) method, FTIR spectra of DTX, Compritol ATO 888, Span 80, Pluronic F127, SLN-DTX, and Blank-SLN were obtained. With a resolution of at least 4 cm1, FTIR spectra were collected over the range of 4000-400 cm1 for 50 scans.

Differential scanning calorimetry (DSC):

Differential scanning calorimetry DSC-60 (Shi-madzu, Kyoto, Japan) was used to produce the thermograms of Compritol ATO 888, Span 80, Pluronic F127, DTX, SLN-DTX, and Blank-SLN. DTX is available as a dry powder, whereas the other samples are liquid. In DSC aluminum crimped pans, samples weighing 4.4 mg, 22 mg, 12.3 mg, 3.2 mg, 2.6 mg, and 9.5 mg each of Compritol ATO 888, Span 80, Pluronic F127, DTX, SLN- DTX, and Blank-SLN were weighed. An empty pan served as the standard. In order to maintain an inert atmosphere during the measurement and avoid an oxidation reaction, DSC was carried out in the 25–400 °C temperature range at a rate of 10 °C/min.

Confocal raman microscopy (CRM):

A confocal Raman spectrometer from Witec GmbH in Germany was used to conduct spectroscopic investigations on the following materials: SLN-DTX, Blank-SLN, Compritol ATO 888, Span 80, and Pluronic F127. The spectra were taken at 0.15 seconds of integration time per point.

Cell culture:

Human breast cancer cells (MCF7), murine embryo fibroblast (NIH- 3T3), and murine breast adenocarcinoma (4T1) cells were cultured in RPMI-1640 or DMEM, supplemented with 10% fetal bovine serum (v:v), penicillin (100 U/mL), and streptomycin (100 U/mL), at 37 °C in a humid environment containing 5% CO2. Human non-tumor mesenchymal cell primary cultures were used with informed consent and with the blessing of the University of Brasilia's human ethics committee (104934/2008). In DMEM, HNTMCs were grown. The following cell tests used cells that were in the logarithmic growth phase. As control cells that weren't cancerous, NIH3-3T3 and HNT- MCs were used.

Cell viability assay:

The colorimetric-based MTT test was used to measure the cytotoxicity. A 96-well plate with 4 103 cells per well of seeded cells was treated overnight. After that, fresh media with various doses of DTX, Blank-SLN, SLN-DTX, or culture medium (negative control) was added to each well for a 24 or 48-hour culture. The culture medium was then changed to one that contained MTT (5 mg/mL), and cells were then incubated for 4 hours at 37 °C. The formazan crystals were then dissolved in each well by adding DMSO after the supernatant was removed. At 595 nm, absorbance was measured. 100% viable, untreated cells were used as the control.By curve fitting the cell viability data, the drug concentration (IC50) at which 50% of the cells' growth was inhibited in contrast to the control sample was determined. Three duplicates of each experiment were carried out.

Cell morphology:

Zeiss, Germany's AxioVision® software and a phase contrast microscope were used to analyze the morphology and confluence of 4T1 cells.

Using Karnovsky overnight fixation, 4T1 cells were fixed 24 hours following treatment (10 g/mL). Samples were post-fixed with osmium tetroxide, dehydrated using graded acetone (30-100%), and rinsed with cacodylate buffer (0,1 M). They were then critical-point dried from liquid CO2 (Balzers, CPD 030, Germany) and gold-sputtered. Scanning electron microscopy was used to examine the cell morphology.

Cell cycle:

Propidium iodide (PI) was used to stain the DNA at various phases for cell cycle analysis, which was detected by flow cytometry. In 24-well cell culture plates, 1 105 cells were plated per well. The 4T1 cells were treated with DTX (10 g/mL) or SLN-DTX for 24 hours. PBS-washed, trypsinized, collected, and centrifuged cells were used. The pellet was preserved in ice-cold, 70% ethanol at 4 °C after being cleaned in PBS. After that, cells were stained using a propidium iodide solution that contained 0.1% Triton X-100, 10 mg/mL RNase A, and 45 mg/mL PI. Using FACS-Calibur (BD Biosciences Co., Franklin Lakes, New Jersey, USA), flow cytometry analysis was carried out after 1 h of incubation at 37 °C in a CO2 incubator.Software called FlowJo single cell analysis was used to evaluate the data.

Cell apoptosis analysis

To distinguish between apoptosis and necrotic cell death brought on by SLN-DTX or DTX, annexin-V staining was used. The incubation period and dose employed in the cell cycle analysis were the same as those that had been administered to the cells. The cells were then taken out, centrifuged, and rinsed with cold PBS. To identify apoptotic and necrotic cell populations, respectively, the cell pellet was resuspended in annexin-binding buffer before being added to Annexin V FITC conjugate and propidium iodide solution. The cells were then measured using a flow cytometer after 15 minutes of incubation at room temperature. Each sample contained 20,000 occurrences in total.

Immunocytochemical staining

4T1 cells were grown on 12-well glass-covered plates for 24 hours before being exposed to SLN-DTX or DTX (10 g/mL). As a control, regular culture media was employed. The cells were fixed with 4% paraformaldehyde for 15 minutes after 24 hours of incubation. After being cleaned with PBS, the cells were permeabilized with 0.5% Triton X-100 for 10 minutes. An anti-tubulin primary antibody was used to stain the cells at a dilution of 1:500 at 4 °C for an overnight period. The tubulin antibody was combined with a goat anti-rabbit IgG that had been conjugated to FITC. The cover slips were put on glass slides after the nucleus had been stained with DAPI (0.1 g/mL) for 7 minutes. A Zeiss Axiophot microscope was used to examine the cells (Carl Zeiss, Jena, Germany

In vitro cellular uptake

By using the analytical method of HPLC, the quantitative analysis of the cellular uptake of DTX by 4T1 cells was carried out. 24-well plates with 105 cells per well were planted with the cells. DTX (100 g/mL) or SLN-DTX were applied to cells for 1, 4, 18, and 24 hours, respectively, at 37 °C with 5% CO2. Cells were washed three times with ice-cold PBS during the incubation period to eliminate any SLN-DTX or DTX that might have remained in the surrounding matrix or on the cell membrane surface. Once all of the cells had been detached by trypsinization (15 min), 800 L of methanol was added to each well, and it was agitated vigorously for 3 min.

In order to guarantee the destruction of nanoparticle structure and the complete DTX dissolution in methanol, each sample was then maintained at 4 °C for 48 hours. Cells were centrifuged at 1000 g for 10 min. at 4 °C after being vortexed for 1 min. In the same manner as described earlier in the "Quantification of DTX by high performance liquid chromatography (HPLC)" section, the supernatant was preserved and subjected to HPLC analysis.

Internalization of SLN-DTX in 4T1 cells

Briefly, 1 106 4T1 cells were seeded, and for 24 hours, they were exposed to SLN-DTX (10 g/mL). After that, cells were fixed with Karnovsky fixative and post-fixed for 1 hour at room temperature with 1% osmium tetroxide containing potassium ferricyanide. Samples were embedded in Epon resin after being dehydrated in grading acetone (30-100%). 5% uranyl acetate was used to stain extremely thin slices. Utilizing a transmission electron microscope (JEOL 1011, Tokyo, Japan) with an accelerating voltage of 80 kV, ultrastructural examinations w

Evaluation of the antitumor activity of the SLN-DTX in vivo:

Balb/c female mice were purchased from the Catholic University of Brasilia (Brasilia, Brazil) when they were 12 weeks old. The University of Brasilia's Animal Research Ethics Committee authorized all the experiments mentioned. A subcutaneous injection of 4T1 cells (4 105 cells per mouse) was made into the left flank. For two weeks, the tumors were allowed to enlarge. Six mice per group were randomly assigned to one of five groups: healthy (tumor-free), PBS, Blank-SLN, free DTX, and SLN-DTX at a fixed dose of 10 mg/kg.

Every four days, the animals received intraperitoneal treatment; there were a total of five applications. As a measure of systemic toxicity, the body weights of mice were tracked [72]. The formula 4/3 (length/2) (width/2)2 was used to compute the tumor size after measuring it with a digital caliper [51].The mice were put to death on day 28, and the tumors and lungs were taken out. Metastatic nodules on the lungs were counted after they had been fixed in Bouin's solution.

Hematology and blood chemistry tests:

For the purpose of performing hemogram and biochemical doses, blood samples were taken. The automated chemistry analyzer (ADVIA 2400, Siemens) and multiple automated hematology analyzer (XZ 2100 Sys-mex equipment) were used to process the hemogram**.**

ELISA:

According to the manufacturer's instructions, an ELISA kit (Sigma, USA) was used to measure the cytokine IL-6 level. In a nutshell, 100 l of standard and mouse plasma were incubated for 45 min at room temperature in duplicate wells. Each well received 100 l of enzyme conjugate reagent following washing, which was followed by incubation. After the reaction was halted, microplate readers were used to measure the samples.

Histopathological and immunohistochemical evaluations :

Hematoxylin and eosin (H&E) was used to evaluate the tumor and lung sections' histology. In the Micra laboratory (in Brasilia, Brazil), immunohistochemical analysis was performed. The tissues were sectioned, fixed in paraffin, and stained with an anti-BCL-2 and anti-Ki-67 antibody from Abcam in Cambridge, Massachusetts, USA. Using a light microscope (Zeiss, Germany), quantification was performed in a blind manner by counting positive cells in 10 fields (400).Immunohistochemical staining was carried out in accordance with the manufacturer's instructions.

Statistical analysis:

Utilizing the program Graph-Pad Prism 5.0, the data were statistically evaluated using the t-test, one- or two-way ANOVA analyses of variance, and Tukey's post-tests. The statistically significant difference was defined as p 0.05. Standard deviation (SD) and mean were used to express quantitative data.

References:

1.Li Y, Jin M, Shao S, Huang W, Yang F, Chen W, et al. Small-sized polymeric micelles incorporating docetaxel suppress distant metastases in the clini- cally-relevant 4T1 mouse breast cancer model. BMC Cancer. 2014;14:329.

2.Hammadi NI, Abba Y, Hezmee MNM, Razak ISA, Jaji AZ, Isa T, et al. Formulation of a sustained release docetaxel loaded cockle shell-derived calcium carbonate nanoparticles against breast cancer. Pharm Res. 2017;34:1193–203.

3.Zhang H, Wang K, Zhang P, He W, Song A, Luan Y. Redox-sensitive micelles assembled from amphiphilic mPEG-PCL-SS-DTX conjugates for the delivery of docetaxel. Colloids Surf B Biointerfaces. 2016. https://doi.org/10.1016/j.colsurfb.2016.02.045.

4.Wang L, Liu Z, Liu D, Liu C, Juan Z, Zhang N. Docetaxel-loaded-lipid- based-nanosuspensions (DTX-LNS): preparation, pharmacokinetics, tissue distribution and antitumor activity. Int J Pharm. 2011;413:194–201.https://doi.org/10.1016/j.ijpharm.2011.04.023.

5.Cho H, Yoon I. Surface-modified solid lipid nanoparticles for oral delivery of docetaxel: enhanced intestinal absorption and lymphatic uptake. Int J Nanomed. 2014;9:495–504.

6.Piccart-Gebhart MJ, Burzykowski T, Buyse M, Sledge G, Carmichael J, Lück HJ, et al. Taxanes alone or in combination with anthracyclines as first-line therapy of patients with metastatic breast cancer. J Clin Oncol. 2008;26:1980–6.

7.Fang G, Tang B, Chao Y, Xu H, Gou J, Zhang Y, et al. Cysteine-functional- ized nanostructured lipid carriers for oral delivery of docetaxel: a perme- ability and pharmacokinetic study. Mol Pharm. 2015;12:2384–95.

8.Mosallaei N, Jaafari MR, Hanafi-Bojd MY, Golmohammadzadeh S, Mal- aekeh-Nikouei B. Docetaxel-loaded solid lipid nanoparticles: preparation, characterization, in vitro, and in vivo evaluations. Pharm Nanotechnol. 2013;9:340–7.

9.Immordino ML, Brusa P, Arpicco S, Stella B, Dosio F, Cattel L. Prepara- tion, characterization, cytotoxicity and pharmacokinetics of liposomes containing docetaxel. J Control Release. 2003;91:417–29.

10.Li X, Du L, Wang C, Liu Y, Mei X, Jin Y. Highly efficient and lowly toxic docetaxel nanoemulsions for intravenous injection to animals. Pharmazie. 2011;66:479–83.

11.Yang M, Ding Y, Zhang L, Qian X, Jiang X, Liu B. Novel thermosensitive polymeric micelles for docetaxel delivery. J Biomed Mater Res Part A. 2007;81:847–57.

12.Sandri G, Motta S, Bonferoni MC, Brocca P, Rossi S, Ferrari F, et al. Chitosan- coupled solid lipid nanoparticles: tuning nanostructure and mucoadhe- sion. Eur J Pharm Biopharm. 2017;110:13–8. https://doi.org/10.1016/j. ejpb.2016.10.010.

13.Zhang L, Zhang N. How nanotechnology can enhance docetaxel therapy. Int J Nanomed. 2013;8:2927–41. https://doi.org/10.2147/ijn.s46921.

14.Cho JBC. Comparison of solid lipid nanoparticles for encapsulating pacli- taxel or docetaxel. J Pharm Invest. 2015;45:625–31.

15.Bhalekar MR, Pokharkar V, Madgulkar A, Patil N, Patil N. Preparation and evaluation of miconazole nitrate-loaded solid lipid nanoparticles for topi- cal delivery. AAPS PharmSciTech. 2009;10:289–96.

16.Liu D, Liu Z, Wang L, Zhang C, Zhang N. Nanostructured lipid carriers as novel carrier for parenteral delivery of docetaxel. Colloids Surf B Biointer- faces. 2011;85:262–9. https://doi.org/10.1016/j.colsurfb.2011.02.038.

17.Aburahma MH, Badr-Eldin SM. Compritol 888 ATO: a multifunctional lipid excipient in drug delivery systems and nanopharmaceuticals. Expert Opin Drug Deliv. 2014;11:1865–83.

18.Karolewicz B, Gajda M, Pluta J, Górniak A. The effect of Pluronic F127 on the physicochemical properties and dissolution profile of lovastatin solid dispersions. J Therm Anal Calorim. 2016;123:2283–90.

19.Fu X, Kong W, Zhang Y, Jiang L, Wang J, Lei J. Novel solid-solid phase change materials with biodegradable trihydroxy surfactants for thermal energy storage. RSC Adv. 2015;5:68881–9.

20.Helgason T, Awad TS, Kristbergsson K, Mcclements DJ, Weiss J. Effect of surfactant surface coverage on formation of solid lipid nanoparticles (SLN). J Colloid Interface Sci. 2009;334:75–81. https://doi.org/10.1016/j. jcis.2009.03.012.

21.Pawar VK, Gupta S, Singh Y, Meher JG, Sharma K, Singh P, et al. Pluronic F-127 stabilised docetaxel nanocrystals improve apoptosis by mitochon- drial depolarization in breast cancer cells: pharmacokinetics and toxicity assessment. J Biomed Nanotechnol. 2015;11:1747–63.

22.Feng L, Mumper RJ. A critical review of lipid-based nanoparticles for taxane delivery. Cancer Lett. 2013;334:157–75.

23.Rahman Z, Zidan AS, Khan MA. Non-destructive methods of characteri- zation of risperidone solid lipid nanoparticles. Eur J Pharm Biopharm. 2010;76:127–37. https://doi.org/10.1016/j.ejpb.2010.05.003.

24.Schwarz C, Mehnert W. Solid lipid nanoparticles (SLN) for controlled drug delivery. II. Drug incorporation and physicochemical characterization. J Microencapsul. 1999;16:205–13.

25.Alexis F, Pridgen E, Molnar LK, Farokhzad OC. Factors affecting the clearance and biodistribution of polymeric nanoparticles. Mol Pharm. 2008;5:505–15.

26.Blanco E, Shen H, Ferrari M. Principles of nanoparticle design for over- coming biological barriers to drug delivery. Nat Biotechnol. 2015;33:941.

27.Moore TL, Rodriguez-Lorenzo L, Hirsch V, Balog S, Urban D, Jud C, et al. Nanoparticle colloidal stability in cell culture media and impact on cel- lular interactions. Chem Soc Rev. 2015;44:6287–305.

28.Anton N, Benoit JP, Saulnier P. Design and production of nanoparticles formulated from nano-emulsion templates—a review. J Control Release. 2008;128:185–99.

29.Estella-Hermoso de Mendoza A, Rayo M, Mollinedo F, Blanco-Prieto MJ. Lipid nanoparticles for alkyl lysophospholipid edelfosine encapsula- tion: development and in vitro characterization. Eur J Pharm Biopharm. 2008;68:207–13.

30.Semete B, Booysen LIJ, Kalombo L, Venter JD, Katata L, Ramalapa B,et al. In vivo uptake and acute immune response to orally administered chitosan and PEG coated PLGA nanoparticles. Toxicol Appl Pharmacol. 2010;249:158–65.

31.Liu Y, Pan J, Feng SS. Nanoparticles of lipid monolayer shell and bio- degradable polymer core for controlled release of paclitaxel: effects of surfactants on particles size, characteristics and in vitro performance. Int J Pharm. 2010;395:243–50.

32.Jansook P, Pichayakorn W, Ritthidej GC. Amphotericin B-loaded solid lipid nanoparticles (SLNs) and nanostructured lipid carrier (NLCs): effect of drug loading and biopharmaceutical characterizations. Drug Dev Ind Pharm. 2018;44:1693–700.

33.Shafique M, Khan MA, Khan WS, Maqsood-Ur-Rehman, Ahmad W, Khan S. Fabrication, characterization, and in vivo evaluation of famotidine loaded solid lipid nanoparticles for boosting oral bioavailability. J Nanomater. 2017. https://doi.org/10.1155/2017/7357150.

34.Qureshi OS, Kim HS, Zeb A, Choi JS, Kim HS, Kwon JE, et al. Sustained release docetaxel-incorporated lipid nanoparticles with improved pharmacokinetics for oral and parenteral administration. J Microencapsul. 2017;34:250–61. https://doi.org/10.1080/02652048.2017.1337247.

35.Albano JM, de Ribeiro LN, Couto VM, Barbosa Messias M, Rodrigues da Silva GH, Breitkreitz MC, et al. Rational design of polymer-lipid nanoparti- cles for docetaxel delivery. Colloids Surf B Biointerfaces. 2019;175:56–64.

36.Krishnamurthi P, Ramalingam HB, Raju K. FTIR studies of hydrogen bond- ing interaction between the hydroxyl and carbonyl liquids. Adv Appl Sci. 2015;6:44–52.

37.Stuart BH. Infrared spectroscopy: fundamentals and applications. Hobo- ken: Wiley; 2005.

38.Jain A, Thakur K, Kush P, Jain UK. Docetaxel loaded chitosan nanoparticles: formulation, characterization and cytotoxicity studies. Int J Biol Macro- mol. 2014;69:546–53.

39.Cipriani P, Ben-amotz D. Characterization of select members of the Taxane family using Raman spectroscopy. J Raman Spectrosc. 2005;36:1052–8.

40.Loiseau A, Boudon J, Mirjolet C, Créhange G, Millot N. Taxane-grafted metal-oxide nanoparticles as a new theranostic tool against cancer: the promising example of docetaxel-functionalized titanate nanotubes on prostate tumors. Adv Healthc Mater. 2017;6:1–10.

41.Gao H, Cao S, Yang Z, Zhang S, Zhang Q, Jiang X. Preparation, characteri- zation and anti-glioma effects of docetaxel-incorporated albumin-lipid nanoparticles. J Biomed Nanotechnol. 2015;11:2137–47.

42.Kaur S, Nautyal U, Singh R, Singh S, Devi A. Nanostructure lipid carrier (NLC): the new generation of lipid nanoparticles. Asian Pac J Health Sci. 2015;2:76–93.

43.Newa M, Bhandari KH, Oh DH, Kim YR, Sung JH, Kim JO, et al. Enhanced dissolution of ibuprofen using solid dispersion with poloxamer 407. Arch Pharm Res. 2008;31:1497–507.

44.Zeng X, Tao W, Mei L, Huang L, Tan C, Feng SS. Cholic acid-functionalized nanoparticles of star-shaped PLGA-vitamin E TPGS copolymer for doc- etaxel delivery to cervical cancer. Biomaterials. 2013;34:6058–67.

45.Naguib YW, Rodriguez BL, Li X, Hursting SD, Williams RO, Cui Z. Solid lipid nanoparticle formulations of docetaxel prepared with high melting point triglycerides: in vitro and in vivo evaluation. Mol Pharm. 2014;11:1239–49.

46.Li X, Wang D, Zhang J, Pan W. Preparation and pharmacokinetics of docetaxel based on nanostructured lipid carriers. J Pharm Pharmacol. 2009;61:1485–92.

47.Sanna V, Roggio AM, Posadino AM, Cossu A, Marceddu S, Mariani A, et al. Novel docetaxel-loaded nanoparticles based on poly(lactide-co-cap- rolactone) and poly(lactide-co-glycolide-co-caprolactone) for prostate cancer treatment: formulation, characterization, and cytotoxicity studies. Nanoscale Res Lett. 2011;6:1–9.

48.Feng SS, Mei L, Anitha P, Gan CW, Zhou W. Poly(lactide)-vitamin E deriva- tive/montmorillonite nanoparticle formulations for the oral delivery of Docetaxel. Biomaterials. 2009;30:3297–306.

49.Mei L, Zhang Y, Zheng Y, Tian G, Song C, Yang D, et al. A novel docetaxel- loaded poly (ε-caprolactone)/Pluronic F68 nanoparticle overcoming multidrug resistance for breast cancer treatment. Nanoscale Res Lett. 2009;4:1530–9.

50.Sunkavalli S, Eedara BB, Janga KY, Velpula A, Jukanti R, Bandari S. Prepara- tion and characterization of docetaxel self-nanoemulsifying powders (SNEPs): a strategy for improved oral delivery. Korean J Chem Eng. 2016;33:1115–24.

51.Zhu D, Tao W, Zhang H, Liu G, Wang T, Zhang L, et al. Docetaxel (DTX)- loaded polydopamine-modified TPGS-PLA nanoparticles as a targeted drug delivery system for the treatment of liver cancer. Acta Biomater. 2016;30:144–54.

52.Xu Z, Chen L, Gu W, Gao Y, Lin L, Zhang Z, et al. The performance of docetaxel-loaded solid lipid nanoparticles targeted to hepatocellular carcinoma. Biomaterials. 2009;30:226–32. https://doi.org/10.1016/j.biomaterials.2008.09.014.

53.Wang H, Li L, Wang P, Wang X, Zhang K, Liu Q. Comparison of photody- namic treatment produced cell damage between human breast cancer cell MCF-7 and its multidrug resistance cell. Photodiagn Photodyn Ther. 2016;16:1–8.

54.Hammadi NI, Abba Y, Hezmee MNM, Razak ISA, Kura AU, Zakaria ZAB. Evaluation of in vitro efficacy of docetaxel-loaded calcium carbonate aragonite nanoparticles (DTX-CaCO3NP) on 4T1 mouse breast cancer cell line. In Vitro Cell Dev Biol Anim. 2017;53:896–907.

55.Hermenean A, Ardelean A. Targeting the cytoskeleton with plant-bioac- tive compounds in cancer therapy. Cytoskelet Struct Dyn Funct Dis. 2017.

56.Zhao X, Qi T, Kong C, Hao M, Wang Y, Li J, et al. Photothermal exposure of polydopamine-coated branched Au–Ag nanoparticles induces cell cycle arrest, apoptosis, and autophagy in human bladder cancer cells. Int J Nanomed. 2018;13:6413.

57.Wang T, Zhu D, Liu G, Tao W, Cao W, Zhang L, et al. DTX-loaded star- shaped TAPP-PLA-b-TPGS nanoparticles for cancer chemical and photo- dynamic combination therapy. RSC Adv. 2015;5:50617–27.

58.Luo Y, Ling Y, Guo W, Pang J, Liu W, Fang Y, et al. Docetaxel loaded oleic acid-coated hydroxyapatite nanoparticles enhance the docetaxel- induced apoptosis through activation of caspase-2 in androgen inde- pendent prostate cancer cells. J Control Release. 2010;147:278–88.

59.Hernández-Vargas H, Palacios J, Moreno-Bueno G. Molecular profiling of docetaxel cytotoxicity in breast cancer cells: uncoupling of aberrant mitosis and apoptosis. Oncogene. 2007;26:2902–13.

60.Sánchez-Moreno P, Boulaiz H, Ortega-Vinuesa JL, Peula-García JM, Aránega A. Novel drug delivery system based on docetaxel-loaded nanocapsules as a therapeutic strategy against breast cancer cells. Int J Mol Sci. 2012;13:4906–19.

61.Patel J, Amrutiya J, Bhatt P, Javia A, Jain M, Misra A. Targeted delivery of monoclonal antibody conjugated docetaxel loaded PLGA nano- particles into EGFR overexpressed lung tumour cells. J Microencapsul. 2018;35:204–17. https://doi.org/10.1080/02652048.2018.1453560.

62.Qiu M, Ouyang J, Sun H, Meng F, Cheng R, Zhang J, et al. Biodegradable micelles based on poly(ethylene glycol)-b-polylipopeptide copolymer: a robust and versatile nanoplatform for anticancer drug delivery. ACS Appl Mater Interfaces. 2017;9:27587–95.

63.Wu CH, Lan CH, Wu KL, Wu YM, Jane WN, Hsiao M, et al. Hepatocel- lular carcinoma-targeted nanoparticles for cancer therapy. Int J Oncol. 2018;52:389–401.

64.Chang DK, Li PC, Lu RM, Jane WN, Wu HC. Peptide-mediated liposomal doxorubicin enhances drug delivery efficiency and therapeutic efficacy in animal models. PLoS ONE. 2013;8:e83239.

65.Kang J, Park JH, Lee HJ, Jo U, Park JK, Seo JH, et al. Caveolin-1 modulates docetaxel-induced cell death in breast cancer cell subtypes through dif- ferent mechanisms. Cancer Res Treat. 2016;48:715.

66.Liang DS, Zhang WJ, Wang AT, Su HT, Zhong HJ, Qi XR. Treating metastatic triple negative breast cancer with CD44/neuropilin dual molecular tar- gets of multifunctional nanoparticles. Biomaterials. 2017;137:23–36. https://doi.org/10.1016/j.biomaterials.2017.05.022.

67.Salgado R, Junius S, Benoy I, Van Dam P, Vermeulen P, Van Marck E, et al. Circulating interleukin-6 predicts survival in patients with metastatic breast cancer. Int J Cancer. 2003;103:642–6.

68.Abana CO, Bingham BS, Cho JH, Graves AJ, Koyama T, Pilarski RT, et al. IL-6 variant is associated with metastasis in breast cancer patients. PLoS ONE. 2017;12:e0181725.

69.Oh K, Lee O, Shon SY, Nam O, Ryu PM, Seo MW. A mutual activation loop between breast cancer cells and myeloid-derived suppressor cells facili- tates spontaneous metastasis through IL-6 trans-signaling in a murine model. Breast Cancer Res. 2013;15:R79.

70.Li GC, Wang ZY. Constitutive expression of RbAp46 induces epithelial– mesenchymal transition in mammary epithelial cells. Anticancer Res BMC Cancer. 2006;26:3555–60.

71.Del Bufalo D, Biroccio A, Leonetti C, Zupi G. Bcl-2 overexpression enhances the metastatic potential of a human breast cancer line. FASEB J. 1997;11:947–53.

72.Du N, Song LP, Li XS, Wang L, Wan L, Ma HY, et al. Novel pH-sensitive nanoformulated docetaxel as a potential therapeutic strategy for the treatment of cholangiocarcinoma. J Nanobiotechnol. 2015;13:17.